Article

Date Palm Cellulose Nanocrystals (CNCs)/Polyamide Composites: Tailoring Morphological, Mechanical, and Thermal Properties

Cintil Jose [1,*], Thoppil Raveendran Anju [2], Abhimanyu Tharayil [3], Patrik Sobolciak [4], Igor Krupa [4], Mariam Al Ali Al Maadeed [4], Hanieh Kargarzadeh [5,*] and Sabu Thomas [3]

1   Department of Chemistry, Newman College, Thodupuzha 685585, Kerala, India
2   Department of Biochemistry, Newman College, Thodupuzha 685585, Kerala, India
3   School of Energy Materials, Mahatma Gandhi University, Kottayam 686560, Kerala, India
4   Center for Advanced Materials, Qatar University, Doha 2713, Qatar
5   Center of Molecular and Macromolecular Studies, Polish Academy of Sciences, Sienkiewicza 112, 90-363 Lodz, Poland
*   Correspondence: cintiljose@gmail.com (C.J.); hanieh.kargar@gmail.com (H.K.)

Abstract: In the present study, polyamide (PA) was successfully reinforced with cellulose nanocrystal (CNC) prepared from date palm leaves using two different techniques, electrospinning and the solution casting method, and a comparative study of these two systems was performed. The morphological, thermal, wetting, and mechanical properties of the nanocomposites were analyzed for CNC content between 0 and 5 wt%. Morphological analyses showed different roughness in the fractured surface of neat PA and its nanocomposites after the addition of CNC. The modified composite is found to have a smooth surface without cracks and showed increased roughness with greater hydrophilicity and thermal stability. The nano-indentation results showed that the highest hardness was obtained at 5% CNC loading for the solution cast composite samples, which could be related to the relatively good CNC dispersion with good filler matrix bonding as evidenced by the morphological characterization. We also observed that the electrospinning technique produced nanocomposites of better thermo-physical properties than the solution cast method. The results point to the prospect of the development of nanocomposite films using date-palm-leaf-derived CNC incorporated in PA for high-performance and advanced material applications such as membranes.

Keywords: cellulose nanocrystal; mechanical properties; nano-indentation; wettability

1. Introduction

The importance given to the notion of a sustainable environment has witnessed remarkable achievements in green technology with the development of various biocomposites from renewable sources. The development of high-performance materials made from natural resources is increasing worldwide and these materials will undoubtedly play a huge role in guiding the research on biocomposites in a new direction. The natural fiber cellulose is considered one of the most important biopolymers in the next-generation material development domain. In recent years, a surge of interest in industrial applications of composites containing cellulose bio-fiber has been observed [1–3].

The flexibility during processing, high stiffness, low cost, and eco-friendly nature make cellulose an attractive material of choice to manufacturers. Both micro and nano cellulose can be effectively used as fillers, and cellulose-reinforced plastic composites are gaining more acceptance in structural applications and other industrial sectors. Cellulose nanofiber (CNF) and cellulose nanocrystals (CNC) were incorporated as reinforcement in different types of polymer matrixes such as polyester [4–6], polylactic acid [7], polypropylene [8], low-density polyethylene [9], starch [10], PVC [11], urea-formaldehyde [12], etc. Among

engineered plastic materials, polyamide (PA) and its composites stand out due to their versatile properties. PA is commercially applied in textile, packaging, and automotive manufacturing due to its excellent mechanical and gas barrier properties. However, the physical and mechanical properties of PA film or fiber depend on its crystalline structure and hydrogen bonding, which are mainly affected by processing conditions [13].

In recent years, many studies have been conducted to prepare PA nanocomposites with organic and inorganic nanofillers to enhance the physical and mechanical properties of the neat PA, such as nanosilica [14], nanoclay [15], TiO_2 [16], carbon nanotube [17], etc. However, the cost of these nanofillers and the recycling of their nanocomposites have caused concerns. Nanocellulose is a bio-based nanomaterial that has attracted significant interest to replace expensive synthetic nanofillers due to the aforementioned properties such as low cost, renewability, lightweight, low density, and strong mechanical properties.

Nanocellulose can be effectively used as filler for PA to increase its mechanical properties, and exploring the possibility of an electrospinning technique for the preparation of PA–cellulose nanocomposites will be an attractive option to produce high-quality composites with versatile properties. Although various aspects of electrospun fibers are reported, many fundamental aspects of the process for different polymer–filler interactions are worthy of further investigation in order to gain a thorough understanding of the process [18,19]. Moreover, PA reinforced with CNC was the subject of a very limited number of studies.

Sobolciak et al. [20] prepared a novel membrane based on co-polyamide 6,12 filled with CNC by the electrospinning technique. They found that the addition of 1 wt% of CNCs improved the Young's modulus by 224% and the tensile strength of the composites by 110%. The PA membrane containing 5 wt% of CNC showed an oil/water separation efficiency of over 98%. In another study, Qua et al. [21] produced PA/CNF nanocomposites via the solution-casting technique. The CNFs were obtained from flax and microcrystalline cellulose using combinations of acid hydrolysis, ball milling, and ultrasound. The produced CNFs from the different feedstock sources were of a similar order with lengths ranging from 21 to 300 nm and diameters between 2 and 22 nm. The mechanical properties of PA/CNFs nanocomposite films were significantly improved with the addition of a low concentration of cellulose nanofibers to the polymer matrix. Sridhara et al. [22] used the same technique to prepare the PA/CNF nanocomposites. They found that an amount of 50 wt% of CNF increased the elastic modulus from 1.5 to 4.2 GPa and the tensile strength from 46.3 to 124 MPa. A lower crystallinity and good thermomechanical stability were observed for the PA/CNF nanocomposites. Aitha et al. [23] used solvent casting to prepare PA/CNC nanocomposite films and studied the effect of CNC on the phase transition of PA. They found that the melting temperature and the crystallinity of PA decreased with the increasing amount of CNC, which was due to an increasing percentage of the γ crystalline form relative to the α crystalline form.

Nanocellulose can be isolated from various cellulose sources and biowastes [24–26]. Date palm leaves are a natural cellulose source that are not realizing their potential, and most of them are not converted into useful products and end up being destroyed. Palm trees exceed 100 million around the globe, which poses an enormous amount of biowaste to be exploited per annum. It is imperative, therefore, to find use in the production of cellulose nanocrystals as a cheap alternative raw material. The objective of the present study was to add value to the cellulosic biomass in date palm leaves by converting it to nanomaterial that can be effectively utilized for the preparation of high-quality nanocomposites using different methodologies. For the preparation of nanocomposites, two different methods, (1) the electrospinning method and (2) the film casting method, were used, and then, a comparative study of these two systems was performed. The novelty of the study lies in its approach of utilizing a value-added product from cellulosic biomass as filler for reinforcing polyamides. In addition, this study is unique in reporting extensive characterization of the morphological, mechanical, and thermal properties of the date-palm-leaf-derived, CNC-reinforced PA nanocomposite using two different preparation methods. This provides

input to the scientific community to extend research for future prospects in industries, especially while targeting more eco-friendly approaches.

2. Materials and Methods

Date palm (*Phoenix dactylifera*) leaves were collected from local farms in Qatar and were used for extracting the fiber. Polyamide 6 with a melt flow rate of 600 g/10 min (275 °C, 5 Kg) was supplied by Polyamide Rhodia Companies. Sigma Aldrich supplied propanol, sodium hydroxide (NaOH), acetic acid (CH_3COOH), sodium chlorite ($NaClO_4$), and sulfuric acid (H_2SO_4). Table 1 shows the chemical composition and physical properties of date palm leaves [27].

Table 1. Chemical composition and physical properties of date palm leaves.

Chemical Composition of Date Palm Leaves		
1	Cellulose(%)	47.14
2	Hemicellulose (%)	16.13
3	Lignin (%)	36.73
4	Total extractive (%)	32.86
5	Ash content (%)	15.2
Physical Properties of Date Palm Leaves		
1	Ignition Temperature (°C)	279
2	Peak Temperature (°C)	467
3	Energetic density (GJ/m^3)	820
4	Fuel value index	53

2.1. Cellulose Nanocrystal Production from Date Palm Leaves

The CNCs were isolated from date palm leaves according to previous publications [28–30]. Dried palm leaves were ground into short fibers and treated with 5 wt% NaOH at a temperature of 110 °C for one hour. The fibers were then washed in water and were bleached using a mixture of NaOH and acetic acid (27 and 78.8 g, respectively) and sodium chlorite solution. The bleaching process was repeated three times. After bleaching, the fibers were thoroughly washed and dried. Then, 270.3 g of water was added to 5.9 g of bleached fiber and mixed until a homogenous dispersion was obtained. Thereafter 529.7 g of sulfuric acid was slowly added to the suspension (65 wt% acid concentration). The cellulose in the acid suspension was then hydrolyzed at 44 °C for 130 min under mechanical stirring. The excess sulfuric acid was removed by repeated cycles of water exchange/centrifugations (5000 rpm) at room temp for 10 min until the supernatant became turbid. After the repeated centrifugation cycles, the suspension containing the CNC was washed in distilled water. Then, the CNC suspension was homogenized using an Ultra-Turax T25 homogenizer and was subjected to ultrasound treatment to ensure proper dispersion of CNC. Finally, the neutralization process was carried out by adding drops of a 1 wt% NaOH solution to the CNC suspension. The suspensions were further stored in a refrigerator at 4 °C.

2.2. Processing of CNC/PA Nanocomposites Film by Electrospinning Method

CNC/PA nanocomposite films were prepared according to the technique proposed by [20]. A NaBond (Shenzhen, China) electrospinning device was used to produce a PA/CNC electrospun fiber mat. A polyamide/propanol solution (10 wt%) was prepared, and different weight percentages of the CNCs were added as reinforcement (1, 2.5, and 5 wt%). The solution was sonicated for 5 min to obtain a homogenous dispersion. For the electrospinning process, the suspensions were loaded into a 5 mL plastic disposable syringe with a stainless steel needle. The needle was connected to the positive terminal of a voltage generator designed to produce a voltage of up to 50 kV DC. A thin aluminum foil

covering a 15 cm diameter copper plate was used as the collector. The plate was grounded and maintained at a working distance of 10 cm. An operating voltage of 14 kV was used and the polymer solution was fed into the needle at a flow rate of 0.5 mL/h and drum speed of 200 RPM by a syringe pump. Then, the fiber mats with an approximate thickness of 50 μm were carefully detached from the aluminum foil for characterization.

2.3. Processing of CNC/PA Nanocomposite Films by Solution Casting

The second batch of CNC/PA nanocomposite films was prepared by a solution casting method. A polyamide/propanol solution (10 wt%) was prepared, and different weight percentages of nanofibrils were added as reinforcement (1, 2.5, and 5 wt%). This solution was also sonicated for 5 min to obtain uniform dispersion. Then, the solution was cast into Teflon molds and the as-prepared films were used for different characterizations.

2.4. Characterization Techniques

2.4.1. Microscopy

Transmission electron microscopy (TEM) (model Philips CM 200) was used to determine the dimensions of the cellulose nanocrystals obtained from the palm fibers. A drop of a diluted suspension (1 wt%) was deposited on the surface of a clean copper grid and coated with a thin carbon film. As for contrast in TEM, the cellulose nanocrystals were negatively stained in a 2 wt% solution of uranyl acetate. The sample was dried at ambient temperature before TEM analysis and the measurement was carried out with an accelerating voltage of 80 kV.

The nanocomposite surface roughness was further analyzed using a NT-MDTs Solver PRO atomic force microscope (AFM). Silicon cantilevers with a typical resonant frequency of 240 kHz and a spring constant of 11.8 N/m were used to acquire images in tapping mode at room temperature under ambient conditions. The scanning rate was around 1–5 Hz. Flattening was applied to the raw images before performing roughness analysis.

Scanning electron microscopy (SEM) was used to observe the surface morphology of the filler and composites. Prior to the experiment, the samples were dried in an oven at 60 °C for 12 h. The samples were then coated with gold using a vacuum sputter coater (model SC 500) to avoid subsequent charging before measurement by SEM. The accelerating voltage used was 20 kV and the imaging was performed in a JEOL JSM-820 model microscope.

2.4.2. Thermogravimetric Analysis (TGA)

The thermal stability of the different samples was determined by TGA measurements performed using a Mettler Toledo Thermogravimetric analyzer (TGA/SDTA 85-F). The amount of sample used for each measurement was 10.0 ± 1.0 mg. All measurements were performed under a nitrogen atmosphere with a gas flow of 100 mL min^{-1} by heating the material from room temperature to 800 °C at a heating rate of 10 °C min^{-1}.

2.4.3. Contact Angle Studies

Contact angle measurements were carried out on a SEO Phoenix instrument. Measurements were carried out with water (triple distilled) on samples of size $1 \times 1 \times 2$ cm^3 at room temperature. The volume of the sessile drop was maintained at 3 μL in all cases using a microsyringe. The contact angle was measured within 45–60 s of the addition of the liquid drop with an accuracy of $\pm 1°$. Measurements were repeated 6 to 10 times with different test pieces of the same sample to check the accuracy. In addition, contact angles were measured with definite time intervals for a single drop, and the measurements were recorded as snapshots.

2.4.4. Fourier Transform Infrared Spectroscopy (FTIR)

Fourier transform infrared spectra were recorded using a Shimadzu IR-470 IR spectrophotometer. Fibers at different stages of preparation and the prepared nanocomposites

were analyzed. Prior to the experiment, samples were dried in an oven at 60 °C for 12 h. The FT-IR spectrum of each sample was obtained in the range of 400–4000 cm^{-1}. The KBr disk (ultrathin pellets) method was used and the experiments were carried out with a resolution of 2 cm^{-1}, and a total of 15 scans were employed for each sample.

2.4.5. Nanoindentation Studies

All the nanoindentation tests in this study were performed using a NanoTest apparatus (Micro Materials, Wrexham, UK). A Berkovich (three sided pyramidal) diamond indenter tip manufactured by Micro Materials was used throughout. Nine symmetrical indentations (in the form of a matrix, 30 mm apart) were made on each specimen. The test coupons were cut from the nanocomposites with approximate dimensions of 15 × 15 × 3 mm. The specimens were then mounted onto the nano-indentation fixture using a suitable adhesive. Nanoindentation results were obtained from at least 10 indentations of 50 μm depth for each sample.

3. Results and Discussions

3.1. Morphology of Cellulosic Nanocrystals (CNC) from Date Palm Leaf

The date palm leaf fiber was subjected to chemical treatment to remove the non-cellulosic constituents. This chemically treated mass, when subjected to acid hydrolysis, revealed a unique morphology, obtaining very fine cellulosic nanocrystals from the fiber. These crystals were observed by TEM to obtain an accurate idea of the shape and size of the cellulose whiskers (Figure 1). TEM analysis of the suspension revealed that the nanocrystals had a needle-like structure, and uranyl acetate staining provided a good contrast between the cellulose crystals and the carbon film. The fibrillated CNC showed a higher surface area and better cross-linking characteristics when used as nano-fillers, as evidenced by the subsequent sections. Two types of aggregation of CNC could be observed from the TEM image; closely spaced crystals and isolated single crystals. The CNC with an average length of 200 nm, a width of 20 nm, and an aspect ratio of 10 was observed.
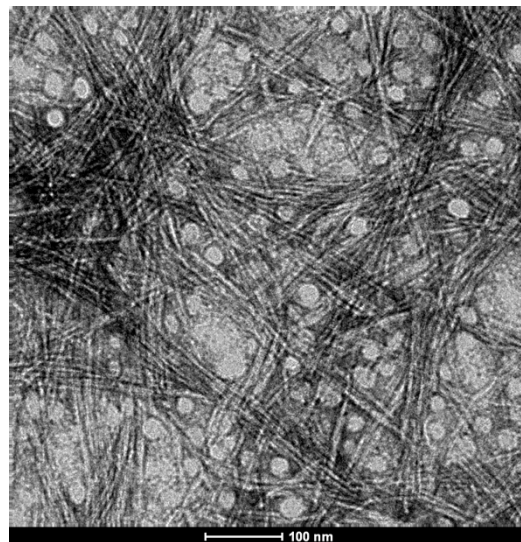

Figure 1. TEM analysis of nanocrystals.

The morphological properties of cellulose nanoparticles are dependent on the source material and the extraction procedures and are important in determining its application [31,32]; the present observation of CNC aggregation pattern is crucial in exploring its application as a nanocomposite.

3.2. Films Prepared by Electrospinning Method

3.2.1. Morphological Analysis of PA/CNC Nanocomposites

The mixtures of PA and CNCs in propanol solvent were homogeneous and clear, and it was easy to electrospin PA and CNC/PA solutions or suspensions when the PA concentration was controlled in the range of 10 wt%. A schematic representation of the nanocomposite formation is given in Figure 2.
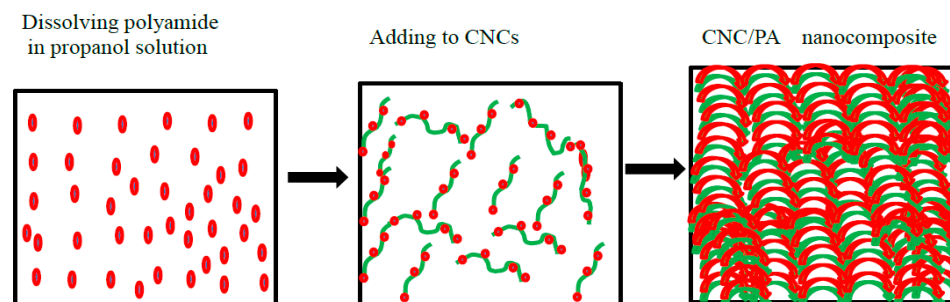

Figure 2. A schematic representation of PA/CNC nanocomposite formation.

Figure 3 shows the atomic force microscopy (AFM) images of neat PA and CNC/PA nanocomposite films prepared by the electrospinning method. It was observed that with an increase in CNC content, the diameter of the produced nanofibers decreased to a small extent. The AFM images confirmed the formation of dense cellulose nanocrystals. The average roughness (R_{avg}) and the root mean square (RMS) roughness (R_{rms}) are two of the most important parameters for the nanocomposite topographies. The average roughness is the arithmetic mean of the surface height (peaks and valleys) deviations with reference to the mean plane of the image [33]. The RMS roughness is the standard deviation of the pixel height data, that is, the deviation of the peaks and valleys from the mean plane, respectively. These values can be used for comparing the membrane roughness [34]. The root means square value of the neat polymer was found to be 18.50 nm and that of the composite containing 1 wt% CNC was found to be 46.47 nm. This clearly shows that the presence of nanofillers increased the roughness values. As the membrane becomes rougher, it provides more space for contact with water drops, resulting in an increased water flux [35]. This can, in turn, increase the wettability or hydrophilicity of the membrane.

Representative SEM images of the polyamide composites containing various concentrations of CNC are shown in Figure 4. The produced PA and PA/CNC nanofibers appear to be smooth and have a uniform thickness. The beads or the bead-on-string structures within the single fibers were also not observed. The viscosity of the electrospinning solution largely determines the diameter and uniformity of the resulting fibers [36]. The average diameters of the electrospun fibers measured from SEM were 3 ± 4.5 μm, 373 ± 256 nm, 270 ± 183 nm, and 170 ± 84 nm for PA, PA/CNC fibers with 1%, 2.5% and 5% CNC content, respectively. We also observed that the surface of the composite fibers was smooth and had no cracks; therefore, it indicated that the CNCs were well dispersed in the PA matrix without significant aggregation. The prepared fibers exhibited regular and homogeneous structures without the presence of any beads. It was considered that the CNCs were negatively charged due to the presence of SO_3^{2-} anions on their surface as a result of the sulfuric acid hydrolysis [37]. Thus, the addition of CNCs was believed to enhance the electrostatic charge density of electrospinning solutions and induce more extensive filament stretching during jet whipping, ultimately resulting in thinner electrospun nanofibers [38,39].
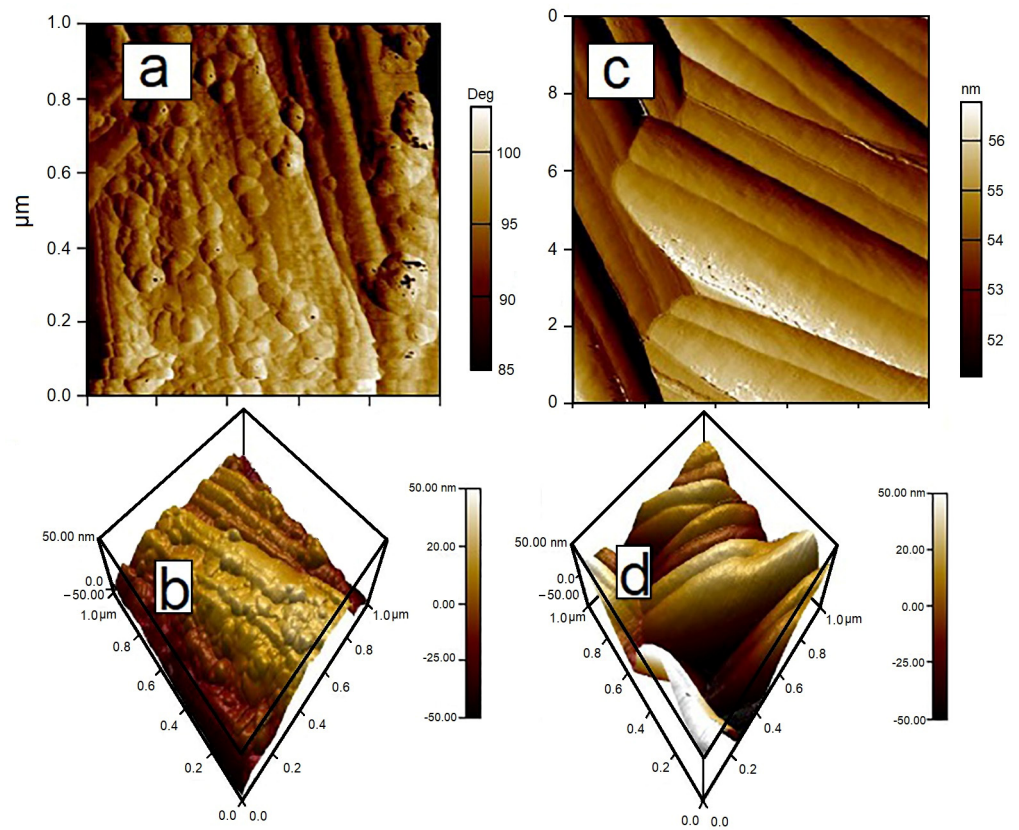
Figure 3. Atomic microscopy images of (**a**,**b**) pristine polyamide and (**c**,**d**) PA with 1 wt% CNC.
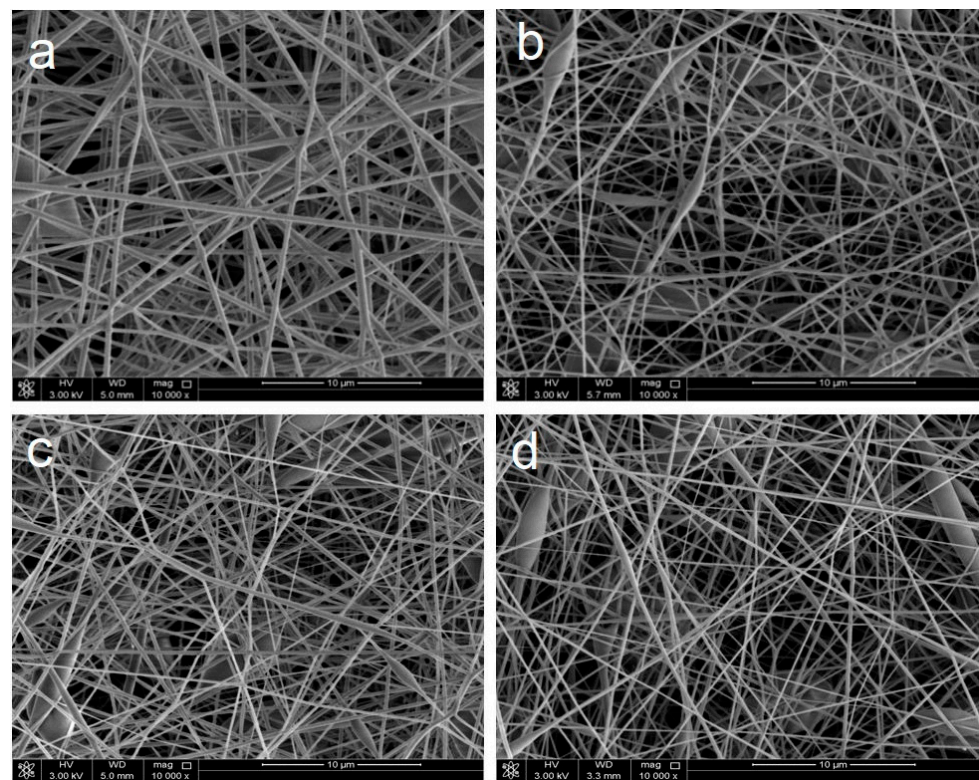

Figure 4. SEM images of (**a**) neat PA, (**b**) PA with 1 wt% CNC, (**c**) PA with 2.5 wt%, and (**d**) PA with 0.5 wt%.

3.2.2. Thermal Behavior of the Electrospun PA/CNC Films

The thermal stability of nanocomposites was investigated by thermogravimetric analysis, and the results are shown in Figure 5. The addition of CNC improved the onset of decomposition temperature for the composites. The thermal degradation of CNCs is a three-step process, the first step is the elimination of water at a temperature of approximately 100–110 °C; the second and the most important step begins at 250 °C, which is caused by the advanced depolymerization of cellulose, dehydration, and decomposition of glycosyl units with the formation of char; and the third step, at a temperature above 425 °C, is assigned to further degradation of charred residue in gaseous products [40]. Similar to some inorganic nanofillers, CNCs enhance the thermal stability of the polymer matrix, as evidenced by higher decomposition values in derivative thermogravimetric (DTG) curve curves. This can be due to the formation of char after CNCs decomposition, which hinders the out-diffusion of the volatile decomposition products of polyamide [41]. The DTG thermograms indicated that the loading of CNCs highly increased the initial decomposition temperatures of the composites, whereas the peak temperatures for the highest weight loss rate were slightly increased. The electrospun PA fibrous mats containing 5 wt% CNCs presented the highest T_{onset} and T_{max}, indicating the most significant improvement in heat resistance, which can be ascribed to the increased crystallinity of electrospun PA/CNC nanocomposites. Thus, the loading of CNCs could improve the thermal stability of PA, possibly due to the intermolecular interactions between PA and CNCs.
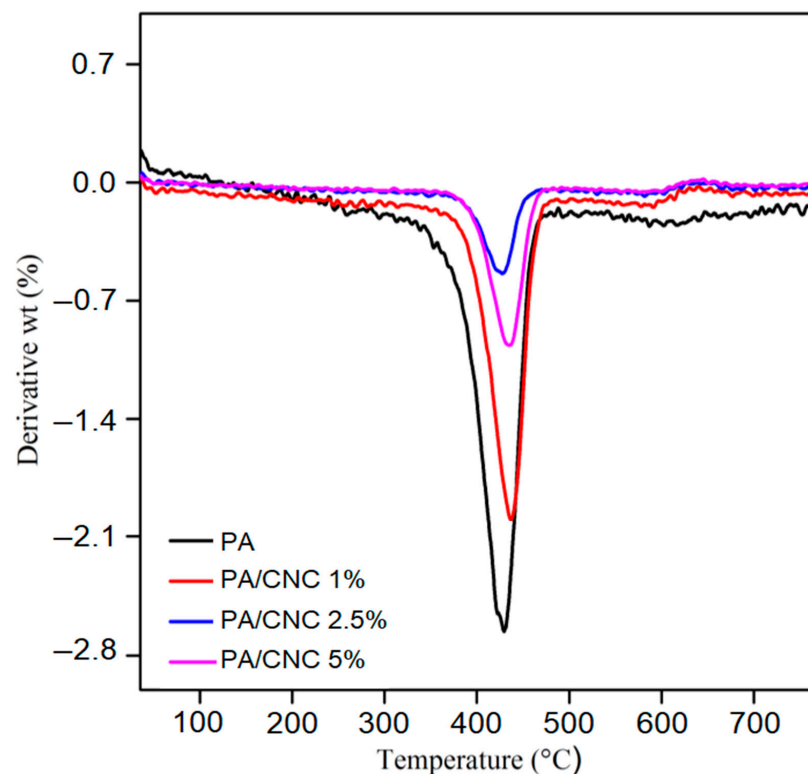

Figure 5. DTG curves of PA and PA/CNC composites.

3.2.3. Surface Wettability of the Electrospun PA/CNC Films

Wettability studies usually involve the measurement of contact angles as the primary data, which indicates the degree of wetting when a solid and liquid interact. Small contact angles (<90°) correspond to high wettability, while large contact angles (>90°) correspond to low wettability. CNC is more hydrophilic than PA, so the addition of CNCs into PA would be expected to improve the wettability of PA. Considering this point, the static water-contact angle measurement was used to evaluate the surface wettability of the nanocomposite films filled with different amounts of CNCs. As shown in Figure 6, with the

addition of CNCs, contact angle values were found to be decreased, which indicated that the composite became more hydrophilic. The addition of CNCs also increased the hydrogen bonding sites to react with moisture. Moreover, nanocelluloses have higher polarity and total surface energy than polyamides [20]. Both characteristics make the nanocomposite film more hydrophilic than the neat polymer film. Surface roughness is an important factor in determining the surface hydrophobicity of materials because a rough surface can trap more air, whose contact angle value is considered to be 180° [42]. The AFM images, along with wettability studies, clearly indicated the increased roughness of the PA/CNC nanocomposite with a lower contact angle and higher hydrophilicity. This again proves the formation of nanocomposites with a smoother void-free surface.
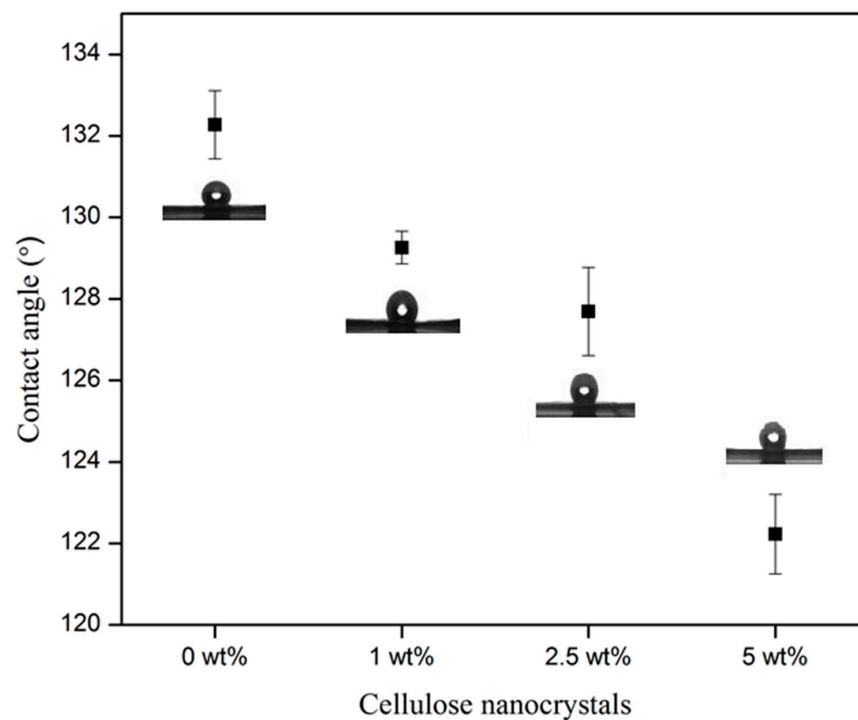

Figure 6. The static water-contact-angle of PA and PA/CNC composites.

3.2.4. Spectroscopic Studies of Electrospun PA/CNC Films

To confirm the inclusion of CNCs in PA/CNC films, all the composites were analyzed by FTIR spectroscopy, as shown in Figure 7. The typical peaks corresponding to PA and CNCs were both observed in the spectra of CNC/PA films, implying the formation of PA/CNC nanocomposites. The absorbance peaks for the CNC were assigned to the wavenumbers of 3342, 1650, and 1164 cm^{-1} for the hydrogen bond O-H stretching, the O-H bending of adsorbed water, and C-O-C asymmetric valence vibration, respectively [39]. As a common feature of polyamide materials, the FT-IR spectrum is dominated by (i) the amide I and amide II bands in the 1500–1700 cm^{-1} region, which are related mainly to the coupled motions of C-O stretching and NH in-plane bending, and (ii) by the NH and CH stretching in the 2800–3300 cm^{-1} region [40,41].

3.2.5. Nanoindentation Studies of Electrospun Nanocomposites

In indentation testing, the hardness is defined as the indentation load divided by the projected contact area. To find the hardness, a measure of the indentation area is needed. The hardness is determined from the peak load and the projected area of contact. Similarly, to obtain the stiffness, the unloading portion of the depth-load curve is analyzed according to a relation that depends on the contact area. Maximum depth, hardness, and stiffness are given in Table 2. The average values of experimental data extracted from the loading/unloading curves from nanoindentation tests are summarized in Table 2. The

load-depth plots of indentations made at a peak indentation load on the four different samples prepared with and without various loadings of CNCs are presented in Figure 8. For the neat PA composite, we observed a stiffness of 136 N/m and a hardness of 2.62 MPa. However, with the addition of CNC, stiffness and hardness are found to be decreased. It is unusual behavior and may be due to the difference in the depth used. With the neat PA composite, the maximum depth was 0.68 µm, but with filler-reinforced composites, it was in the micrometer range. The nanocomposite with 5 wt.% of CNC showed higher stiffness and hardness compared to the nanocomposites with 1 and 2.5 wt% CNC content. The enhancement in mechanical properties could be due to the difference in fiber diameters. As is shown in Figure 4, the PA fiber with 5 wt% CNC has a thinner diameter. The reduction in fiber diameter probably improves the crystallinity and molecular orientation of both PA and CNC, leading to improve mechanical properties of the nanocomposites. However, the value for PA/CNC with 5 wt% is still lower than the value for neat PA. In the case of films prepared by the solution casting technique, the CNC reinforced composites showed a gradual increase in mechanical properties with filler content.
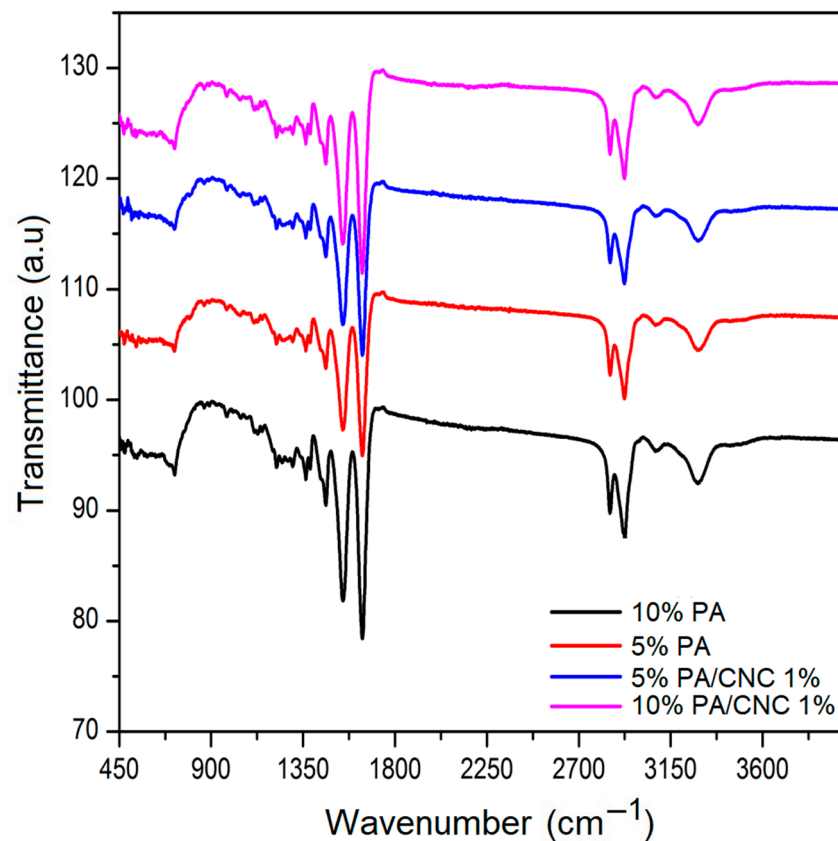

Figure 7. FTIR of neat PA and PA nanocomposites at different loading of CNCs.

Table 2. Summary of nanoindentation test results for the films prepared by electrospinning technique.

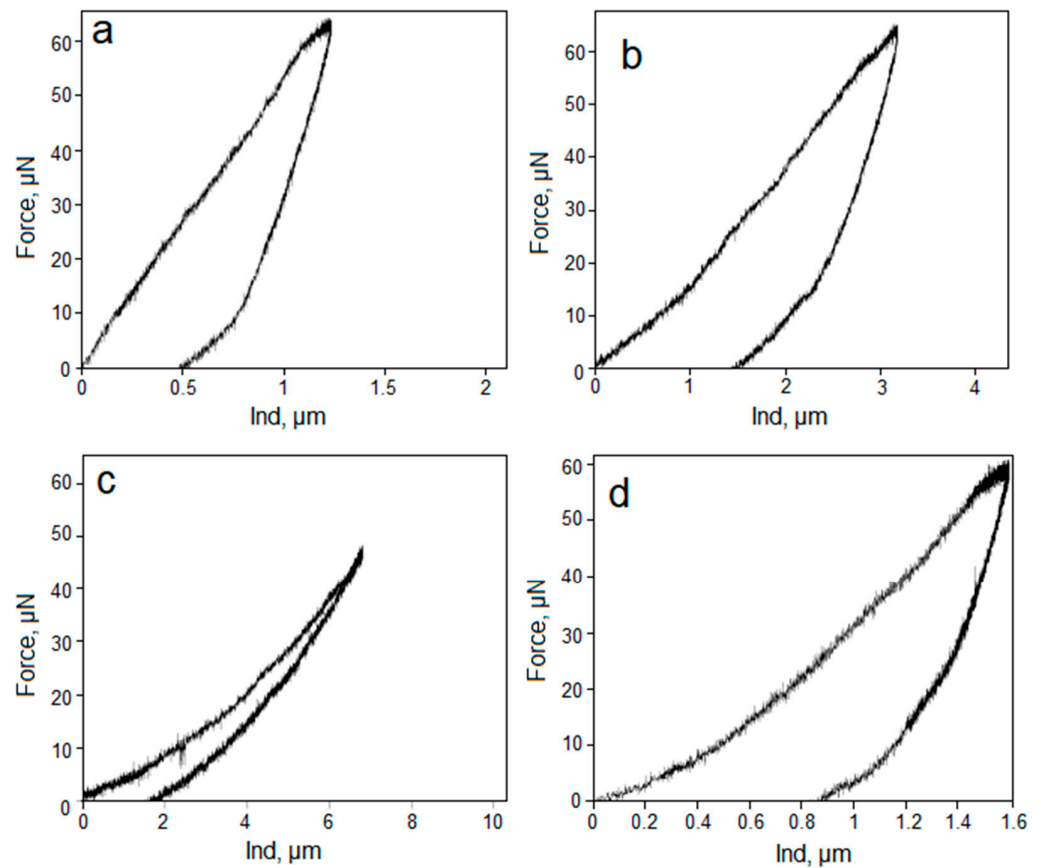| Sample	Max Depth (µm)	Stiffness (N/m)	Hardness
Neat PA	0.68	136.84 ± 5.50	2.62 ± 0.15 MPa
1 wt% CNC	1.97	65.00 ± 2.00	452.00 ± 3.00 kPa
2.5 wt% CNC	1.15	14.87 ± 1.00	103.00 ± 2.50 kPa
5 wt% CNC	0.92	139.00 ± 4.00	1.54 ± 0.10 MPa

Figure 8. Nanoindentation studies of (**a**) Neat PA and (**b**) PA with 1 wt% CNC, (**c**) 2.5 wt%, (**d**) 5 wt% CNC.

3.3. Films Prepared by Solution Casting

3.3.1. Morphological Analysis of CNC/PA Nanocomposites

The surface morphology of the thin films prepared by solution casting is shown in Figure 9, and it shows the dispersion state of CNC at various filler loadings. The microscopic aspects of the fracture surface of the composite samples revealed a good explanation for the improvement in properties. The maximum improvement in mechanical properties was observed at 5 wt% of filler; where effective stress transfer occurred at this optimum loading, the matrix particles are seen sticking to the filler surfaces. When there is a nice dispersion of the fillers, crack propagation will be prevented by the neighboring fibrils. In addition to this, an appropriate aspect ratio and the high surface area of nanofibrils lead to stronger bonding between fibrils and matrix.

The topographic features, as well as the phase characteristics of surfaces in all composites, were investigated using AFM in the phase contrast tapping mode. AFM images of the surface characteristics of the nanocomposite are given in Figure 10. The most uniform dispersion was observed at 5 wt% concentration, and the nanofillers were found to be dispersed homogeneously throughout the matrix without any aggregation. When there is a uniform dispersion of fillers, there is stronger bonding between fibrils and matrix, which leads to better properties.
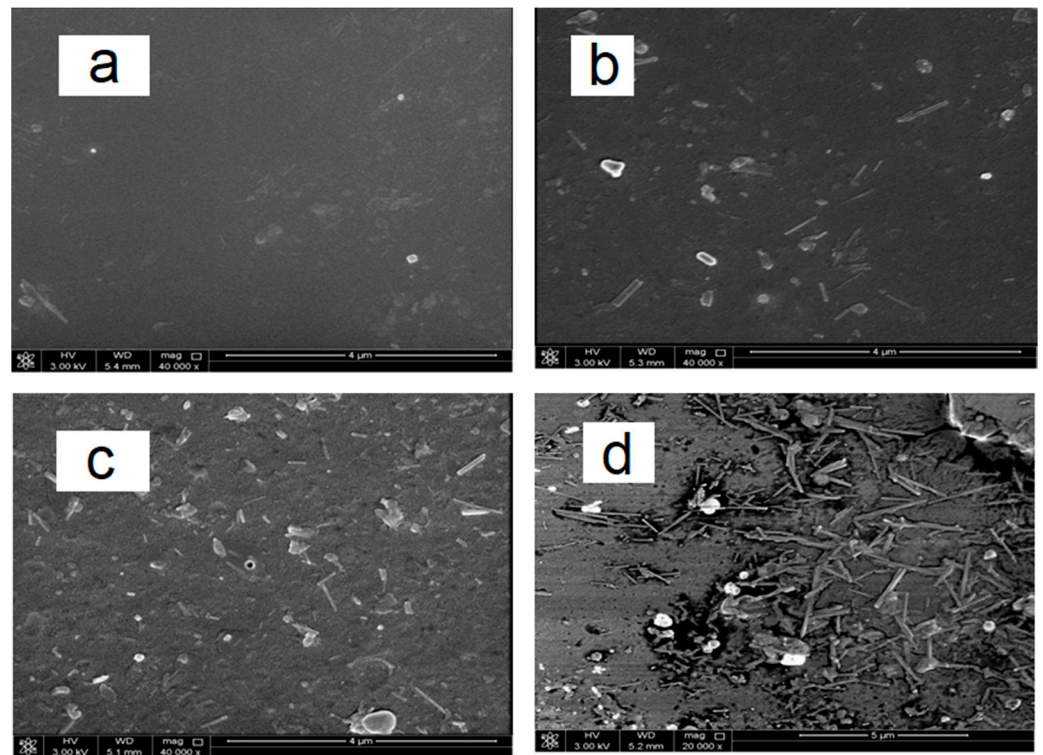
Figure 9. SEM images of (**a**) Neat PA and (**b**) PA with 1 wt% CNC, (**c**) PA with 2.5 wt% CNC, (**d**) PA with 5 wt% CNC.
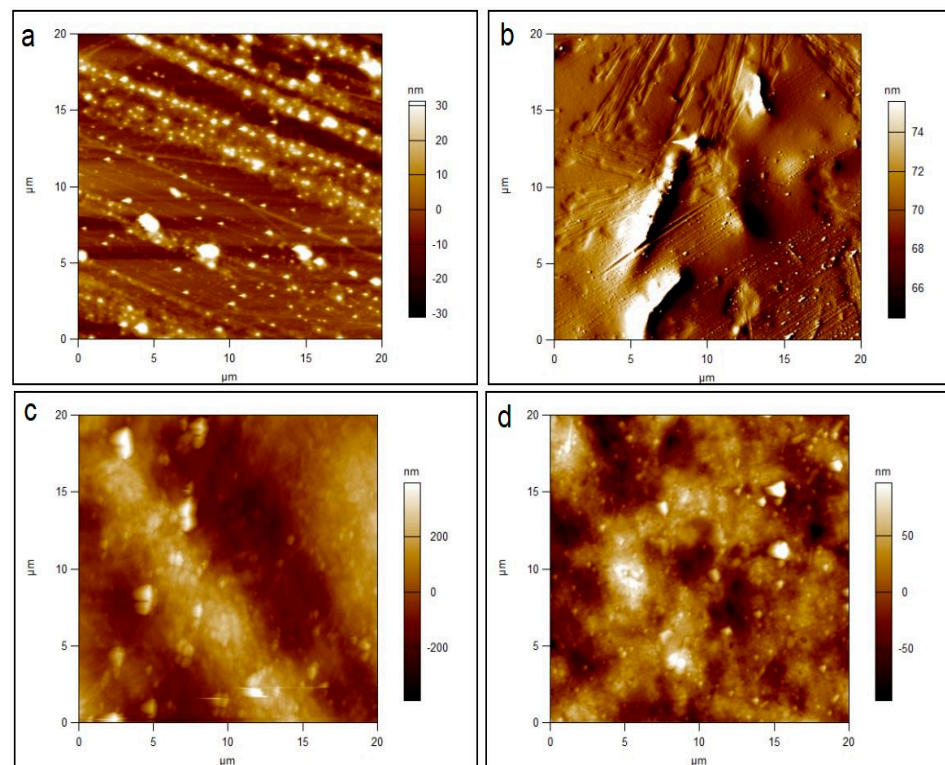

Figure 10. Atomic microscopy images of (**a**) neat PA and (**b**) PA with 1 wt%, (**c**) 2.5 wt%, and (**d**) 5 wt% CNC.

3.3.2. Thermal Behavior of the CNC/PA Films by Solution Casting

Figure 11 shows the thermogravimetric analysis of PA/CNC nanocomposites. The initial degradation at 110 °C is due to the removal of bound water present in all samples. All composites were found to be stable up to 400 °C. It was also observed that the addition of CNC slightly improves the thermal stability of the nanocomposites. However, the thermal stability decreased with increasing CNC content. Generally, the addition of nanocellulose into hydrophilic composites improved the thermal properties of the composites. Because PA is a hydrophilic polymer, therefore, an improvement in thermal stability of the nanocomposites is expected. This improvement could be due to the PA-CNC strong interaction via hydrogen, which required more energy for cleavage and, thus, improved the resistance to decomposition. The thermal properties of nanocellulose polymer composites are discussed comprehensively in Gan et al. [43].
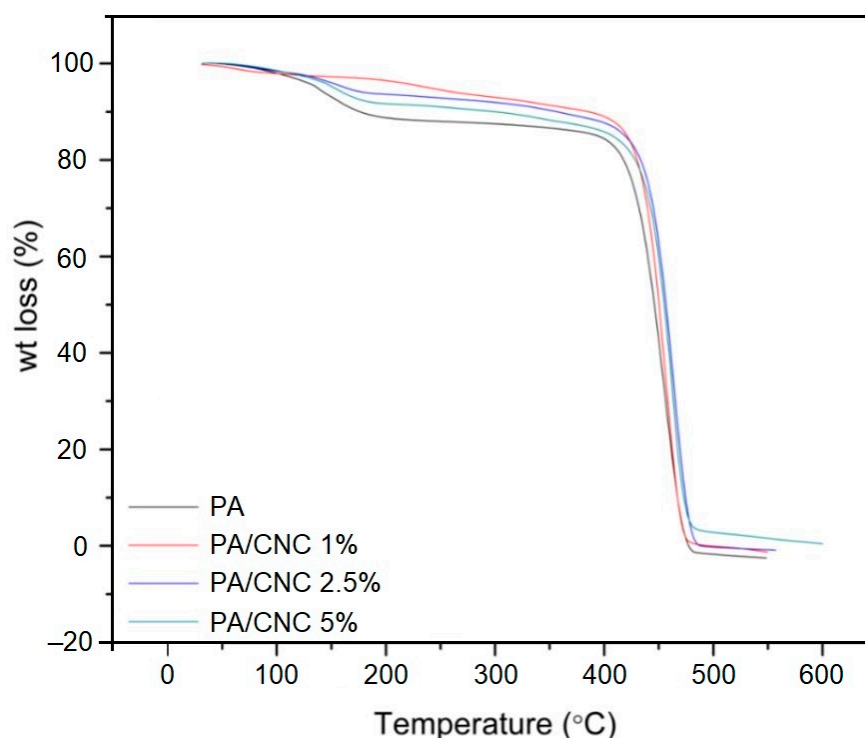

Figure 11. Thermogravimetric analysis of neat PA and PA/CNC nanocomposites.

3.3.3. Surface Wettability of CNC/PA Films by Solution Casting

An appropriate experimental technique for quantifying the surface properties of solids is the measurement of contact angles of liquids on solid surfaces. The interfacial properties between a liquid and a polymer component are characterized by the surface energies of each phase and the contact angle between them. The wetting properties were calculated and given in Figure 12. The nanocomposites showed wetting behavior with the addition of CNC, and the decrease in contact angle value is in perfect correlation with the increase in filler concentration. The hydrophilic nature of the composites is found to increase with the addition of fillers.

3.3.4. Spectroscopic Studies of CNC/PA Films by Solution Casting

The chemical nature of the neat PA and CNC/PA composites was explored using FTIR studies. Due to the small loading level of nanocrystals into the PA matrix, the signature spectra do not significantly differ. The characteristic FTIR spectra for neat PA and CNC/PA composite samples are shown in Figure 13. The major absorption band located at 3298 cm^{-1} can be attributed to N–H stretching mode vibrations from the PA matrix. The presence of two main bands at 2931 and 2860 cm^{-1} is due to asymmetric and symmetric stretching

vibrations of H–C–H groups [44]. The absorption band at 1635 cm^{-1} represents amide I (C–O stretching vibrations), whereas the stretching frequency observed at 1540 cm^{-1} corresponds to amide II (a combination of N–H bending vibration and stretching vibration of the C–N bond) and/or CH$_2$ asymmetric deformation [45,46].
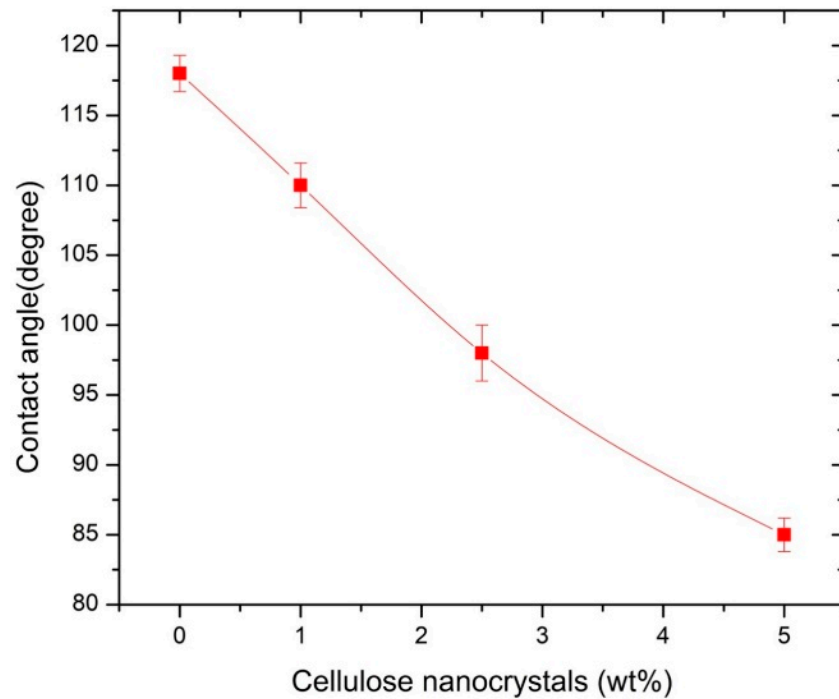

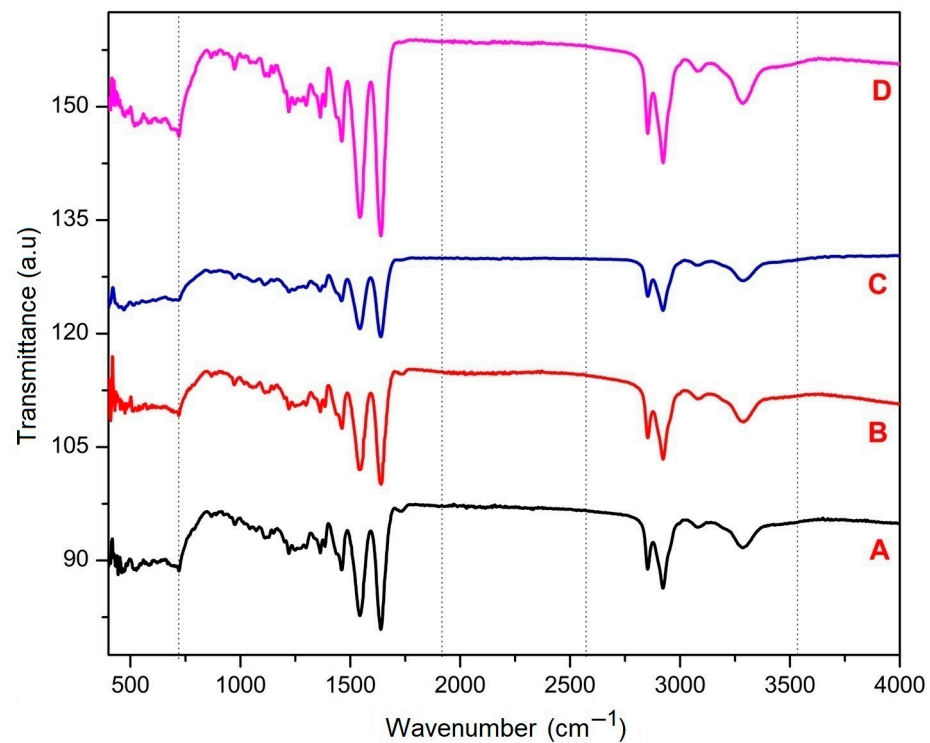**Figure 12.** The static water-contact-angle of PA and CNC/PA composites.

Figure 13. FTIR of PA and PA/CNC nanocomposites at different loadings of CNCs; (**A**) PA, (**B**) 1% CNC, (**C**) 2.5% CNC, (**D**) 5% CNC.

3.3.5. Nanoindentation Studies of PA/CNC Films by Solution Casting

With an increase in the layer silicate reinforcement, the material's resistance to nanoindentation is found to increase. The neat PA has the highest indentation depth (1.21 μm); hence, it has the lowest hardness (15 GPa). The depth at peak load for 1 wt% CNC sample is 343 nm, which is lower than that of other unreinforced neat PA samples, and it exhibits a hardness value of 158 MPa. The hardness value indicates the ability of the material's resistance to plastic deformation. From the results, it can be seen that CNC has a clear reinforcement effect on the PA matrix. This is revealed by the increased hardness of all the PA/CNC samples when compared to neat PA. The increase in hardness can be related to a nano-effect; a change in the properties of the matrix caused by the high surface area of nanoparticles [47]. This is clearly displayed in Table 3, whereby the hardness and modulus of all the nanocomposite samples are significantly higher than the neat PA samples. The mechanisms of improvement in the nano hardness for the PA matrix can be explained as the positive effect of a high aspect ratio. Figure 14 illustrates the difference between the un-reinforced PA sample and PA/CNC nanocomposite samples. The addition of the "high aspect ratio" CNC into the PA matrix leads to an increase in hardness (decrease in indentation depth) in comparison to the neat PA.

Table 3. Summary of nanoindentation test results for composite films prepared by solution casting.

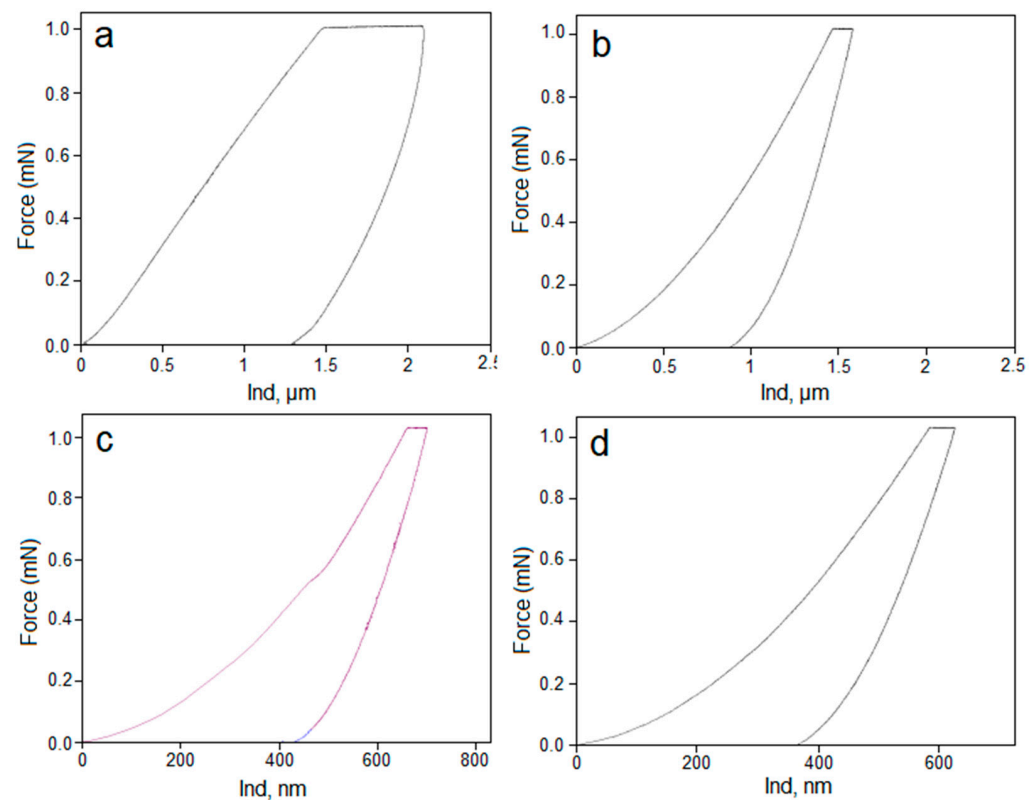| Sample	Max Depth	Stiffness (kN/m)	Hardness (MPa)
Neat PA	1.21 μm	1.72 ± 0.50	15 ± 2.00
1 wt% CNC	343 nm	6.36 ± 1.50	158 ± 3.00
2.5 wt% CNC	443 nm	6.12 ± 1.00	158 ± 3.00
5 wt% CNC	350 nm	6.73 ± 1.00	161 ± 2.00

Figure 14. Nano indentation studies of (**a**) Neat PA, (**b**) PA with 1% CNC, (**c**) 2.5%, (**d**) 5% CNC.

4. Conclusions

We extracted CNC from date palm leaves and used them as reinforcement to prepare PA/CNC nanocomposites. The nanocomposites were produced via the electrospinning technique and solution casting method and their mechanical, thermal, and morphological properties, as well as their hydrophobicity, were compared. Both applied techniques are simple and show promise in the mass production of PA/CNC nanocomposites. The extracted CNC had an average length of 200 nm, a width of 20 nm, and an aspect ratio of 10. The morphological and wettability studies indicated the increased roughness of the electrospun PA/CNC nanocomposite with a lower contact angle and higher hydrophilicity, which proved the formation of nanocomposites with a smoother void-free surface. The PA/CNC cast films had smooth surfaces without cracks and showed similar wetting behavior to the electrospun nanocomposites. The hydrophilic nature of both nanocomposites was found to increase with the addition of CNC. The neat electrospun PA had a stiffness of 136 N/m and a hardness of 2.62 MPa. However, with the addition of CNC, stiffness and hardness were decreased. In the case of casting nanocomposites, the addition of the CNC into the PA matrix led to an increase in hardness and a decrease in indentation depth in comparison to the neat PA. The thermal stability of PA/CNC nanocomposites prepared in both casting and electrospinning techniques showed a slight improvement due to the strong filler–matrix interaction, which required higher thermal energy for cleavage and to decompose. It was also found that the viscosity of the electrospinning solution largely determined the diameter and uniformity of the resulting fibers. Thus, the addition of CNCs enhanced the electrostatic charge density of electrospinning solutions and ultimately resulted in thinner electrospun nanofibers. Between the two methods adopted for CNC-PA nanocomposite preparation, the electrospinning technique produced nanocomposites with better thermo-physical properties. These results indicate that the incorporation of cellulose nanocrystals derived from date palm leaves into polyamide is a promising method for improving the thermo-physical performance of the PA-CNC nanocomposites. Further studies need to be conducted to identify the mechanical and crystalline properties of the nanocomposite. The PA/CNC nanocomposite has many potential applications as filters for the separation of sub-micron particles, as reinforcing fillers in composite materials, as wound-dressing and tissue scaffolding materials for medical uses, and as controlled release materials for agricultural and pharmaceutical uses.

Author Contributions: Conceptualization, M.A.A.A.M. and S.T.; data curation, P.S.; formal analysis, T.R.A.; funding acquisition, S.T.; investigation, C.J.; methodology, C.J.; project administration, M.A.A.A.M. and S.T.; resources, T.R.A. and S.T.; software, A.T. and I.K.; supervision, T.R.A. and S.T.; visualization, C.J. and T.R.A.; writing—original draft, C.J., A.T., P.S. and I.K.; writing—review and editing, H.K. All authors have read and agreed to the published version of the manuscript.

Data Availability Statement: Data sharing is not applicable to this article.

Conflicts of Interest: The authors declare no conflict of interest.

References

1. Babu, R.P.; Oconnor, K.; Seeram, R. Current progress on bio-based polymers and their future trends. *Prog. Biomater.* **2013**, *2*, 8. [CrossRef] [PubMed]
2. Kargarzadeh, H.; Mariano, M.; Huang, J.; Lin, N.; Ahmad, I.; Dufresne, A.; Thomas, S. Recent developments on nanocellulose reinforced polymer nanocomposites: A review. *Polymer* **2017**, *132*, 368–393. [CrossRef]
3. Kargarzadeha, H.; Huang, J.; Lin, N.; Ahmad, I.; Mariano, M.; Dufresne, A.; Thomas, S.; Gałeski, A. Recent developments in nanocellulose-based biodegradablepolymers, thermoplastic polymers, and porous nanocomposites. *Prog. Polym. Sci.* **2018**, *87*, 197–227. [CrossRef]
4. Zaghloul, M.M.Y.; Mohamed, Y.S.; El-Gamal, H. Fatigue and tensile behaviors of fiber-reinforced thermosetting composites embedded with nanoparticles. *J. Compos. Mater.* **2019**, *53*, 709–718. [CrossRef]

5.   Kargarzadeh, H.; Sheltami, R.M.; Ahmad, I.; Abdullah, I.; Dufresne, A. Cellulose nanocrystal: A promising toughening agent for unsaturated polyester nanocomposite. *Polymer* **2015**, *56*, 346–357. [CrossRef]

6.   Zaghloul, M.Y.M.; Zaghloul, M.M.Y.; Zaghloul, M.M.Y. Developments in polyester composite materials–An in-depth review on natural fibres and nano fillers. *Compos. Struct.* **2021**, *278*, 114698. [CrossRef]

7.   Yu, F.; Fei, X.; He, Y.; Li, H. Poly(lactic acid)-based composite film reinforced with acetylated cellulose nanocrystals and ZnO nanoparticles for active food packaging. *Int. J. Biol. Macromol.* **2021**, *186*, 770–779. [CrossRef]

8.   Sunny, T.; Pickering, K.L. Cellulose nanocrystal treatment of aligned short hemp fibre mats for reinforcement in polypropylene matrix composites. *Cellulose* **2021**, *28*, 8429–8444. [CrossRef]

9.   Kaboorani, A.; Gray, N.; Hamzeh, Y.; Abdulkhani, A.; Shirmohammadli, Y. Tailoring the low-density polyethylene—thermoplastic starch composites using cellulose nanocrystals and compatibilizer. *Polym. Test.* **2021**, *93*, 107007. [CrossRef]

10.   Kargarzadeh, H.; Johar, N.; Ahmad, I. Starch biocomposite film reinforced by multiscale rice husk fiber. *Compos. Sci. Technol.* **2017**, *151*, 147–155. [CrossRef]

11.   Sheltami, R.M.; Kargarzadeh, H.; Abdullah, I. Effects of silane surface treatment of cellulose nanocrystals on the tensile properties of cellulose-polyvinyl chloride nanocomposite. *Sains Malays.* **2015**, *44*, 801–810. [CrossRef]

12.   Khanjanzadeh, H.; Behrooz, R.; Bahramifar, N.; Pinkl, S.; Gindl-Altmutter, W. Application of surface chemical functionalized cellulose nanocrystals to improve the performance of UF adhesives used in wood based composites—MDF type. *Carbohydr. Polym.* **2019**, *206*, 11–20. [CrossRef] [PubMed]

13.   Rafique, F.Z.; Vasanthan, N. Crystallization, Crystal Structure, and Isothermal Melt Crystallization Kinetics of Novel Polyamide 6/SiO2 Nanocomposites Prepared Using the Sol–Gel Technique. *J. Phys. Chem.* **2014**, *118*, 9486–9495. [CrossRef] [PubMed]

14.   Kausar, A. Polyamide/nanosilica nanocomposite: A chronicle of design and high-tech progressions. *Mater. Res. Innov.* **2022**, *26*, 52–63. [CrossRef]

15.   Zhang, X.; Loo, L.S. Morphology and mechanical properties of a novel amorphous polyamide/nanoclay nanocomposite. *J. Polym. Sci. Part B Polym. Phys.* **2008**, *46*, 2605–2617. [CrossRef]

16.   Lee, H.S.; Im, S.J.; Kim, J.H.; Kim, H.J.; Min, B.R. Polyamide thin-film nanofiltration membranes containing TiO2 nanoparticles. *Desalination* **2008**, *219*, 48–56. [CrossRef]

17.   Mahmood, N.; Islam, M.; Hameed, A.; Saeed, S. Polyamide 6/multiwalled carbon nanotubes nanocomposites with modified morphology and thermal properties. *Polymers* **2013**, *5*, 1380–1391. [CrossRef]

18.   Zuppolini, S.; Cruz-Maya, I.; Guarino, V.; Borriello, A. Optimization of polydopamine coatings onto poly−ε−caprolactone electrospun fibers for the fabrication of bio-electroconductive interfaces. *J. Funct. Biomater.* **2020**, *11*, 19. [CrossRef]

19.   Thakkar, S.; Misra, M. Electrospun polymeric nanofibers: New horizons in drug delivery. *Eur. J. Pharm. Sci.* **2017**, *107*, 148–167. [CrossRef]

20.   Sobolčiak, P.; Tanvir, A.; Popelka, A.; Moffat, J.; Mahmoud, K.A.; Krupa, I. The preparation, properties and applications of electrospun co-polyamide 6,12 membranes modified by cellulose nanocrystals. *Mater. Des.* **2017**, *132*, 314–323. [CrossRef]

21.   Qua, E.H.; Hornsby, P.R.; Sharma, H.S.S.; Lyons, G. Preparation and characterisation of cellulose nanofibres. *J. Mater. Sci.* **2011**, *46*, 6029–6045. [CrossRef]

22.   Sridhara, P.K.; Masso, F.; Olsén, P.; Vilaseca, F. Strong polyamide-6 nanocomposites with cellulose nanofibers mediated by green solvent mixtures. *Nanomaterials* **2021**, *11*, 2127. [CrossRef] [PubMed]

23.   Aitha, S.; Vasanthan, N. Effect of cellulose nanocrystals on crystallization, morphology and phase transition of polyamide 6. *Compos. Interfaces* **2019**, *27*, 371–384. [CrossRef]

24.   Khanjanzadeh, H.; Park, B.-D. Optimum oxidation for direct and efficient extraction of carboxylated cellulose nanocrystals from recycled MDF fibers by ammonium persulfate. *Carbohydr. Polym.* **2020**, *251*, 117029. [CrossRef] [PubMed]

25.   Khanjanzadeh, H.; Park, B.-D. Characterization of Carboxylated Cellulose Nanocrystals from Recycled Fiberboard Fibers Using Ammonium Persulfate Oxidation. *J. Korean Wood Sci. Technol.* **2020**, *48*, 231–244. [CrossRef]

26.   Kargarzadeh, H.; Ioelovich, M.; Ahmad, I.; Thomas, S.; Dufresne, A. Methods fro extraction of nanocellulose from various sources. In *Hanbook of Nanocellulose and Cellulose Nanocomposites*; Kargarzadeh, H., Ed.; Wiley: Weinheim, Germany, 2017; pp. 1–49.

27.   Nasser, R.A.; Salem, M.Z.M.; Hiziroglu, S.; Al-Mefarrej, H.A.; Mohareb, A.S.; Alam, M.; Aref, I.M. Chemical Analysis of Different Parts of Date Palm (*Phoenix dactylifera* L.) Using Ultimate, Proximate and Thermo-Gravimetric Techniques for Energy Production. *Energies* **2016**, *9*, 374. [CrossRef]

28.   Sheltami, R.M.; Abdullah, I.; Ahmad, I.; Dufresne, A.; Kargarzadeh, H. Extraction of cellulose nanocrystals from mengkuang leaves (*Pandanus tectorius*). *Carbohydr. Polym.* **2012**, *88*, 772–779. [CrossRef]

29.   Brito, B.S.L.; Pereira, F.; Putaux, J.-L.; Jean, B. Preparation, morphology and structure of cellulose nanocrystals from bamboo fibers. *Cellulose* **2012**, *19*, 1527–1536. [CrossRef]

30.   Lu, P.; Hsieh, Y. Preparation and characterization of cellulose nanocrystals from rice straw. *Carbohydr. Polym.* **2012**, *87*, 564–573. [CrossRef]

31.   Elazzouzi-Hafraoui, S.; Nishiyama, Y.; Putaux, J.-L.; Heux, L.; Dubreuil, F.; Rochas, C. The shape and size distribution of crystalline nanoparticles prepared by acid hydrolysis of native cellulose. *Biomacromolecules* **2008**, *9*, 57–65. [CrossRef]

32.   Silvério, H.A.; Neto, W.P.F.; Dantas, N.O.; Pasquini, D. Extraction and characterization of cellulose nanocrystals from corncob for application as reinforcing agent in nanocomposites. *Ind. Crop. Prod.* **2013**, *44*, 427–436. [CrossRef]

33. Mbuli, B.S.; Nxumalo, E.N.; Mhlanga, S.D.; Krause, R.W.; Pillay, V.L.; Oren, Y.; Linder, C.; Mamba, B.B. Development of antifouling polyamide thin-film composite membranes modified with amino-cyclodextrins and diethylamino-cyclodextrins for water treatment. *J. Appl. Polym. Sci.* **2014**, *131*, 1–10. [CrossRef]
34. Adeniyi, A.; Onyango, M.; Bopape, M. Impact of nodular structure in characterization of three thin film composite membranes made from 1, 2-benzisothiazol-3 (2H)-one, sodium salt. *J. Mater. Environ. Sci.* **2019**, *10*, 213–224.
35. Raposo, M.; Ferreira, Q.; Ribeiro, P. A Guide for Atomic Force Microscopy Analysis of Soft- Condensed Matter. *Mod. Res. Educ. Top. Microsc.* **2007**, *1*, 758–769.
36. Ghobeira, R.; Asadian, M.; Vercruysse, C.; Declercq, H.; De Geyter, N.; Morent, R. Wide-ranging diameter scale of random and highly aligned PCL fibers electrospun using controlled working parameters. *Polymer* **2018**, *157*, 19–31. [CrossRef]
37. Jordan, J.H.; Easson, M.W.; Condon, B.D. Alkali hydrolysis of sulfated cellulose nanocrystals: Optimization of reaction conditions and tailored surface charge. *Nanomaterials* **2019**, *9*, 1232. [CrossRef] [PubMed]
38. Kumar, A.; Sinha-Ray, S. A review on biopolymer-based fibers via electrospinning and solution blowing and their applications. *Fibers* **2018**, *6*, 45.
39. Gong, X.; Kalantari, M.; Aslanzadeh, S.; Boluk, Y. Interfacial interactions and electrospinning of cellulose 524 nanocrystals dispersions in polymer solutions: A review. *J. Dispers. Sci. Technol.* **2020**, *43*, 945–977. [CrossRef]
40. Rosace, G.; Castellano, A.; Trovato, V.; Iacono, G.; Malucelli, G. Thermal and flame retardant behaviour of cotton fabrics treated with a novel nitrogen-containing carboxyl-functionalized organophosphorus system. *Carbohydr. Polym.* **2018**, *196*, 348–358. [CrossRef]
41. Ng, H.-M.; Sin, L.T.; Bee, S.-T.; Tee, T.-T.; Rahmat, A.R. Review of Nanocellulose Polymer Composite Characteristics and Challenges. *Polym.-Plast. Technol. Eng.* **2017**, *56*, 687–731. [CrossRef]
42. Shim, M.H.; Kim, J.; Park, C.-H. The effects of surface energy and roughness on the hydrophobicity of woven fabrics. *Text. Res. J.* **2014**, *4*, 1268–1278. [CrossRef]
43. Gan, P.G.; Sam, S.T.; Bin Abdullah, M.F.; Omar, M.F. Thermal properties of nanocellulose-reinforced composites: A review. *J. Appl. Polym. Sci.* **2020**, *137*, 48544. [CrossRef]
44. Rogulska, M.; Kultys, A.; Olszewska, E. New thermoplastic poly(thiourethane-urethane) elastomers based on hexane-1,6-diyl diisocyanate (HDI). *J. Therm. Anal. Calorim.* **2013**, *114*, 903–916. [CrossRef]
45. De Campos Vidal, B.; Mello, M.L.S. Collagen type I amide I band infrared spectroscopy. *Micron* **2011**, *42*, 283–289. [CrossRef] [PubMed]
46. Balan, V.; Mihai, C.-T.; Cojocaru, F.-D.; Uritu, C.-M.; Dodi, G.; Botezat, D.; Gardikiotis, I. Vibrational spectroscopy fingerprinting in medicine: From molecular to clinical practice. *Materials* **2019**, *12*, 2884. [CrossRef] [PubMed]
47. Tharayil, A.; Banerjee, S.; Kar, K.K. Dynamic mechanical properties of zinc oxide reinforced linear low density polyethylene composites. *Mater. Res. Express* **2019**, *6*, 055301. [CrossRef]